JOC Article

Bicorannulenyl: Stereochemistry of a $C_{40}H_{18}$ Biaryl Composed of Two Chiral Bowls

David Eisenberg,[†] Alexander S. Filatov,[‡] Edward A. Jackson,[§] Mordecai Rabinovitz,[†] Marina A. Petrukhina,[‡] Lawrence T. Scott,[§] and Roy Shenhar*,[†]

Institute of Chemistry and The Lise Meitner-Minerva Center for Computational Quantum Chemistry, The Hebrew University of Jerusalem, Jerusalem 91904, Israel, Department of Chemistry, State University of New York, Albany, New York 12222, and Department of Chemistry, Merkert Chemistry Center, Boston College, Chestnut Hill, Massachusetts 02467-3860

roys@chem.ch.huji.ac.il

Received February 19, 2008

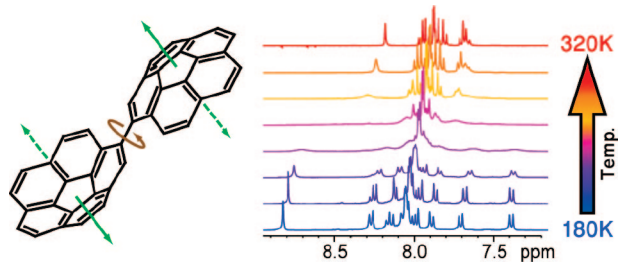

The bicorannulenyl molecule is composed of two chiral bowls tethered by a single bond in a helical fashion. This simple combination of two chiral motifs gives rise to rich dynamic stereochemistry, where 12 conformers interconvert through bowl inversions and central bond rotation, and enantiomerizations occur via multistep processes. Interestingly, 8 out of 10 transition states are chiral, giving rise to mostly chiral enantiomerization pathways, where the molecule changes chirality without passing through an achiral conformation. However, analysis of the stereochemical landscape by DFT calculations and variable temperature NMR spectroscopy reveals that the energetically most favorable enantiomerization pathway passes through one of the two achiral transition states. Single-crystal X-ray diffraction corroborates the DFT results and provides information on packing modes of bicorannulenyl molecules in the solid state that have not been seen previously for other buckybowls.

Introduction

Curved geodesic polyarenes have appealed to chemists ever since the discovery of fullerenes.[1] Bowl-shaped polycyclic aromatic hydrocarbons that can be mapped onto the surface of C_{60} hold a promise for better syntheses of fullerenes,[2] offer a unique arena for studying the effect of curvature on aromaticity[3] and exhibit unique reactivity, such as supramolecular aggregation in the anionic state[4] and complexation of transition metals.[5]

The dynamic stereochemistry of corannulene (**1**) has been extensively researched in experiment and theory over the past 15 years. Structure **1** is the smallest curved fragment of C_{60}, undergoing rapid bowl inversion at room temperature.[6] Various aspects of the inversion dynamics have been studied, including the quadratic curvature-energy correlation[7] and the dependence

[†] The Hebrew University of Jerusalem.
[‡] State University of New York, Albany.
[§] Boston College.

(1) For recent reviews, see: Sygula, A.; Rabideau, P. W. In *Carbon-Rich Compounds: From Molecules to Materials*; Haley, M. M., Tykwinski, R. R., Eds.; Wiley-VCH: Weinheim, Germany, 2006; pp 529−565. Wu, Y.-T.; Siegel, J. S. *Chem. Rev.* **2006**, *106*, 4843. Tsefrikas, V. M.; Scott, L. T. *Chem. Rev.* **2006**, *106*, 4868.

(2) Scott, L. T.; Boorum, M. M.; McMahon, B. J.; Hagen, S.; Mack, J.; Blank, J.; Wegner, H.; de Meijere, A. *Science* **2002**, *295*, 1500. Scott, L. T. *Angew. Chem.* **2004**, *116*, 5102. Scott, L. T. *Angew. Chem., Int. Ed.* **2004**, *43*, 4994.

(3) Xu, S.-H.; Zhang, M.-Y.; Zhao, Y.-Y.; Chen, B.-G.; Zhang, J.; Sun, C.-C. *J. Mol. Struct. (THEOCHEM)* **2006**, *760*, 87. Mascal, M. *J. Org. Chem.* **2007**, *72*, 4323. Shenhar, R.; Beust, R.; Hagen, S.; Bronstein, H. E.; Willner, I.; Scott, L. T.; Rabinovitz, M. *J. Chem. Soc., Perkin Trans.* **2002**, *2*, 449.

(4) Ayalon, A.; Sygula, A.; Cheng, P.-C.; Rabinovitz, M.; Rabideau, P. W.; Scott, L. T. *Science* **1994**, *265*, 1065. Aprahamian, I.; Eisenberg, D.; Hoffman, R. E.; Sternfeld, T.; Matsuo, Y.; Jackson, E. A.; Nakamura, E.; Scott, L. T.; Sheradsky, T.; Rabinovitz, M. *J. Am. Chem. Soc.* **2005**, *127*, 9581. Treitel, N.; Sheradsky, T.; Peng, L.; Scott, L. T.; Rabinovitz, M. *Angew. Chem.* **2006**, *118*, 3351. Treitel, N.; Sheradsky, T.; Peng, L.; Scott, L. T.; Rabinovitz, M. *Angew. Chem., Int. Ed.* **2006**, *45*, 3273.

(5) Petrukhina, M. A.; Scott, L. T. *Dalton Trans.* **2005**, 2969. Petrukhina, M. A. *Coord. Chem. Rev.* **2007**, *251*, 1690.

(6) Scott, L. T.; Hashemi, M. M.; Bratcher, M. S. *J. Am. Chem. Soc.* **1992**, *114*, 1920.

10.1021/jo800359z CCC: $40.75 © 2008 American Chemical Society
Published on Web 05/28/2008

of curvature on charge,[8] position of substituents[7] and heterosubstitution.[9]

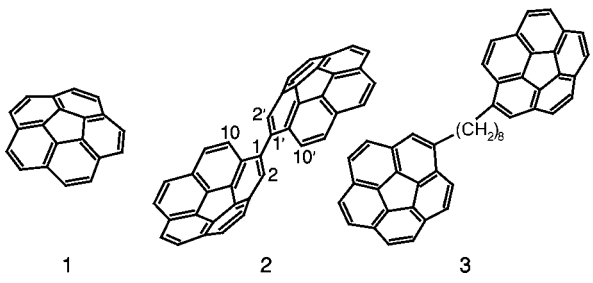

Dimers and oligomers of corannulene display promising capabilities for conduction[10] and hosting, along with complex stereochemistry.[11] For example, the concave-concave conformation of a bis-corannulene "clamshell" recently synthesized by Sygula et al. is capable of embracing a C_{60} molecule, forming a host−guest complex in solution and in the solid state.[12]

Bicorannulenyl (**2**) is made of two corannulene bowls linked by a single covalent bond. The chirality of **2** can be viewed as a combination of two "chiral motifs": the asymmetry of each curved, monosubstituted corannulenyl bowl and the helical chirality about the central σ-bond, analogous to *ortho*-substituted biphenyls.[13] When combined, these structural elements afford rich dynamic stereochemistry, with many combinations of bowls and twists about the central bond. Unlike dicorannulenyloctane (**3**), whose stereochemistry has been studied in the past,[11a] the bowls in bicorannulenyl are conjugated. This introduces new considerations into the stereodynamic energetics. In this work, the dynamic stereochemistry of bicorannulenyl is unraveled by a combined experimental and theoretical approach.[14]

Results and Discussion

Temperature-dependent ^{1}H NMR spectra of **2** reveal a dynamic process in the molecule (Figure 1). At room temperature and above, a single set of peaks consisting of one singlet and eight doublets is observed, corresponding to hydrogen 2 and the other eight hydrogens, respectively. As temperature is lowered the resonances broaden, and when the spectrum finally sharpens near 200 K, three sets of peaks are evident rather than one. The three sets represent three separate diastereomers, as shown by 2D-NMR experiments (COSY and NOESY).

To account for the dynamic NMR results, we have analyzed the stereochemical space of bicorannulenyl. The chirality arising from the curvature of each bowl was denoted as P or M,

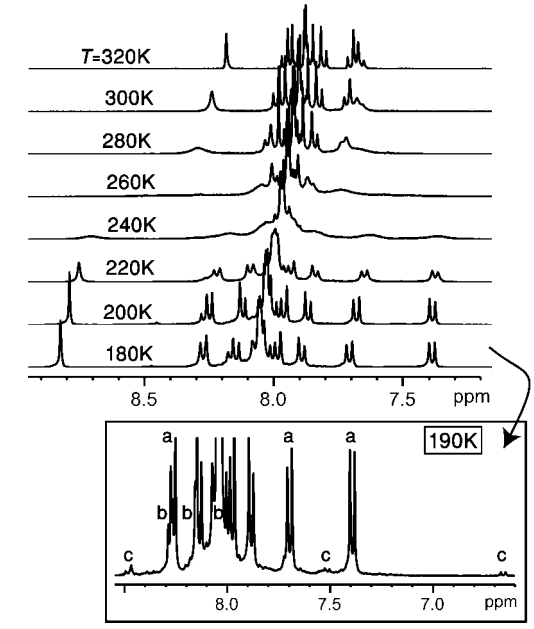

FIGURE 1. Dynamic ^{1}H NMR spectra of bicorannulenyl. The inset shows a blown up spectrum recorded at 190 K with representative absorptions from the three sets (**a**, **b**, **c**) denoted.

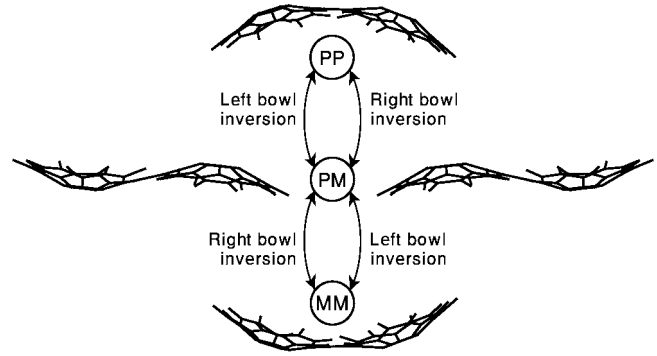

FIGURE 2. Combinations of bowl-shaped corannulenyl moieties and transitions between them, with the dihedral angle between the bowls fixed at 180° (note that at this dihedral angle the PM and MP combinations are identical).

according to previously suggested nomenclature.[15,16] The torsion angle was defined as the dihedral angle ϕ between C2−C1−C1′−C2′:[17] a right-handed helix (S) at $0° < \phi < 180°$, and a left-handed one (R) at $-180° < \phi < 0°$.

Four combinations of bowls exist in **2**, denoted PP, MM, PM and MP (the latter two are *meso* forms), interconverting by bowl inversions as shown in Figure 2. The value of the torsion angle is required to understand how these combinations relate to each other in space. MM and PP are enantiomers when their ϕ is of opposite sign; PM and MP are also enantiomers under these conditions, except at 0° and 180°, where they are identical. In all other cases, each pair of conformers is diastereomeric.

The right and left helices are separated by energy barriers for bond rotation, where the energy reaches maxima at torsion angles close to 0° and 180° (Figure 3). These barriers arise from

(7) Seiders, T. J.; Baldridge, K. K.; Grube, G. H.; Siegel, J. S. *J. Am. Chem. Soc.* **2001**, *123*, 517.
(8) Sygula, A.; Rabideau, P. W. *J. Mol. Struct. (THEOCHEM)* **1995**, *333*, 215.
(9) Priyakumar, U. D.; Sastry, G. N. *J. Org. Chem.* **2001**, *66*, 6523.
(10) Salcedo, R. *J. Mol. Struct. (THEOCHEM)* **1996**, *369*, 189.
(11) (a) Shabtai, E.; Hoffman, R. E.; Cheng, P.-C.; Bayrd, E.; Preda, D. V.; Scott, L. T.; Rabinovitz, M. *J. Chem. Soc., Perkin Trans.* **2000**, 2, 129. (b) Sygula, A.; Sygula, R.; Ellern, A.; Rabideau, P. W. *Org. Lett.* **2003**, *5*, 2595. (c) Zhechkov, L.; Heine, T.; Seifert, G. *J. Phys. Chem. A* **2004**, *108*, 11733. (d) Wu, Y.-T.; Hayama, T.; Baldridge, K. K.; Linden, A.; Siegel, J. S. *J. Am. Chem. Soc.* **2006**, *128*, 6870. (e) Jackson, E. A.; Scott, L. T. Unpublished results.
(12) Sygula, A.; Fronczek, F. R.; Sygula, R.; Rabideau, P. W.; Olmstead, M. M. *J. Am. Chem. Soc.* **2007**, *129*, 3842.
(13) First discovered in 2,2′-dinitro-6,6′-dicarboxylic acid-biphenyl: Christie, G. H.; Kenner, J. H. *J. Chem. Soc.* **1922**, *121*, 614.
(14) A brief attempt to resolve the stereodynamics of neutral bicorannulenyl and to study its reduction pattern appears in: Shabtai, E. From cyclophanes to fullerenes: Three dimensional carbon rich anions. Ph.D. dissertation, The Hebrew University of Jerusalem, Israel, 1999.
(15) Petrukhina, M. A.; Andreini, K. W.; Peng, L.; Scott, L. T. *Angew. Chem.* **2004**, *116*, 5594. Petrukhina, M. A.; Andreini, K. W.; Peng, L.; Scott, L. T. *Angew. Chem., Int. Ed* **2004**, *43*, 5477.
(16) See Supporting Information for more details.
(17) An alternative definition of the torsion angle in **2** designates ω as the angle between the calculated mean planes of the two bowls.

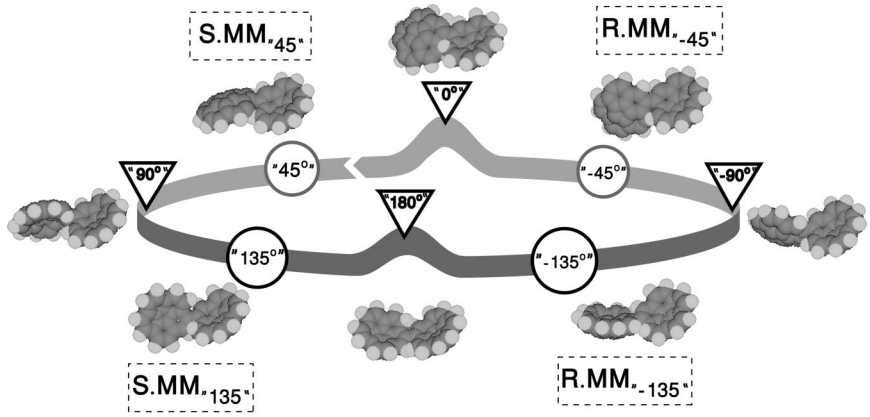

FIGURE 3. Circular coordinate for bond rotation, with the bowls arbitrarily fixed in the MM conformations. Notice that the bowl on the right is fixed, and the bowl on the left rotates. The expected values of the dihedral angles of stable conformations and of transition states are denoted in circles and triangles, respectively. In the dashed boxes the full names are given for the conformations: S or R for the helix (determined according to the helix nomenclature), M or P for the bowls and the dihedral angle in subscript (positive for S and negative for R).

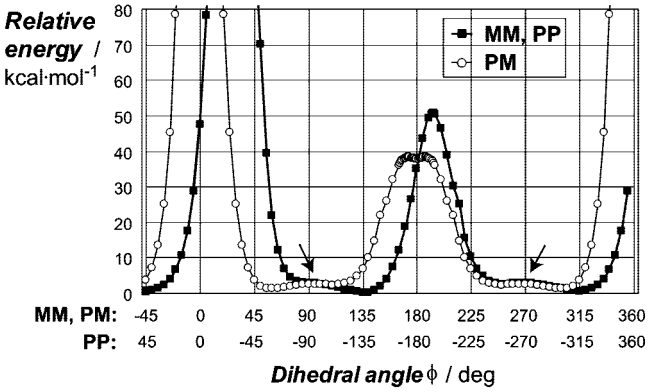

FIGURE 4. Energy scan along ϕ with frozen bowl geometries, for upper and lower decks (MM + PP, based on $S.PP_{46}$) and the middle deck (PM, based on $S.PM_{60}$). Arrows mark the conjugation loss barriers.

steric repulsion, as at 0° H2/H2′ (and H10′/H10) are in the greatest proximity, and at 180° H2/H10′ (and H10/H2′) collide. In addition, one should expect small energy barriers near ±90° due to loss of π-conjugation when the bowls are perpendicular to each other, as in biphenyl.[18] A 360° sweep of the torsion angle in a given species thus passes through four stable conformations and four energy barriers (Figure 3): two due to steric hindrance and two due to conjugation loss. In MM and PP, the steric hindrance barriers are expected to occur at ϕ angles deviating from 0° and 180°, because these transition states are asymmetric, unlike in PM_0 (C_s) and PM_{180} (C_i).

To confirm this analysis, the energy was scanned along a full 360° cycle of the torsion angle ϕ, starting from a fully optimized structure at $\phi = 44°$ for the S.PP and at $\phi = 58°$ for the S.PM (minima structures, see below) and continuing with single point calculations, where the bowls' internal structure is held fixed and ϕ is varied by 5° or less (Figure 4).[16] As expected, there are two large steric hindrance energy barriers, near $\phi = 0°$ and 180°, which are exaggerated in magnitude due to the partly optimized structures employed in the scan. In addition, two small barriers rising to 1−2 kcal·mol^{-1} are observed at $\phi = \pm 90°$, which arise from conjugation loss. The PM_0 and PM_{180} steric hindrance barriers include a minute double hump (less than 1 kcal·mol^{-1} in the single point scan, symmetrically centered around 0° and 180°), which arises from the fact that in the "rigid bowls" model used for the angle scan, the hydrogen pairs on each side of the tether collide at two different torsion angles.[19]

When the two degrees of freedom in the molecule, bowl inversion (Figure 2) and bond rotation (Figure 3), are combined, the resulting stereodynamics can be sketched upon a "stereodynamics map" as shown in Figure 5. The map presents all possible conformations and the transition states for their interconversions, their relative energies and exact dihedral angles, as determined using DFT calculations.[20] An important observation is that pairs of enantiomers are located always on the *same "face" of the cylinder wall* (front/rear as the map is drawn) on opposite "sides" (left/right). The map also outlines the various enantiomerization pathways. For example, $S.PM_{122}$ can enantiomerize to $R.MP_{-122}$ in a single rotation about the central bond, while an enantiomerization of $S.PP_{44}$ from the upper "deck" to $R.MM_{-44}$ in the lower one requires at least two bowl inversions and one bond rotation.

The vertical coordinate, which represents bowl inversion, is drawn as wide "curtains" rather than as single lines to emphasize the negligible disturbance of the conjugation loss barriers to the bond rotation motion at the transition state even at low temperatures. A ϕ-scan performed with one bowl locked in its inversion transition state geometry revealed a conjugation loss barrier that was as low as that calculated with full geometry optimization.[16] Thus, the isomerization from $S.PP_{44}$ to $S.PM_{122}$,

(18) Almenningen, A.; Bastiansen, O.; Fernholt, L.; Cyvin, B. N.; Cyvin, S. J.; Samdal, S. *J. Mol. Struct.* **1985**, *128*, 59.

(19) The "double hump" feature can be either real or an artifact of the restricted optimization procedure. Nevertheless, the calculated energies of the partially optimized PM_0 and PM_{180} provide reasonable lower limit estimations for the respective barriers.

(20) *Gaussian '03*, Revision B.05; Frisch, M. J.; Trucks. G. W.; Schlegel, H. B.; Scuseria, G. E.; Robb, M. A.; Cheeseman, J. R.; Montgomery, J. A., Jr.; Vreven, T.; Kudin, K. N.; Burant, J. C.; Millam, J. M.; Iyengar, S. S.; Tomasi, J.; Barone, V.; Mennucci, B.; Cossi, M.; Scalmani, G.; Rega, N.; Petersson, G. A.; Nakatsuji, H.; Hada, M.; Ehara, M.; Toyota, K.; Fukuda, R.; Hasegawa, J.; Ishida, M.; Nakajima, T.; Honda, Y.; Kitao, O.; Nakai, H.; Klene, M.; Li, X.; Knox, J. E.; Hratchian, H. P.; Cross, J. B.; Bakken, V., Adamo, C.; Jaramillo, J.; Gomperts, R.; Stratmann, R. E.; Yazyev, O.; Austin, A. J.; Cammi, R.; Pomelli, C.; Ochterski, J. W.; Ayala, P. Y.; Morokuma, K.; Voth, G. A.; Salvador, P.; Dannenberg, J. J.; Zakrzewski, V. G.; Dapprich, S.; Daniels, A. D.; Strain, M. C.; Farkas, O.; Malick, D. K.; Rabuck, A. D.; Raghavachari, K.; Foresman, J. B.; Ortiz, J. V.; Cui, Q.; Baboul, A. G.; Clifford, S.; Cioslowski, J.; Stefanov, B. B.; Liu, G.; Liashenko, A.; Piskorz, P.; Komaromi, I.; Martin, R. L.; Fox, D. J.; Keith, T.; Al-Laham, M. A.; Peng, C. Y.; Nanayakkara, A.; Challacombe, M. ; Gill, P. M. W.; Johnson, B.; Chen, W.; Wong, M. W.; Gonzalez, C.; Pople, J. A. Gaussian, Inc.: Wallingford, CT, 2003.

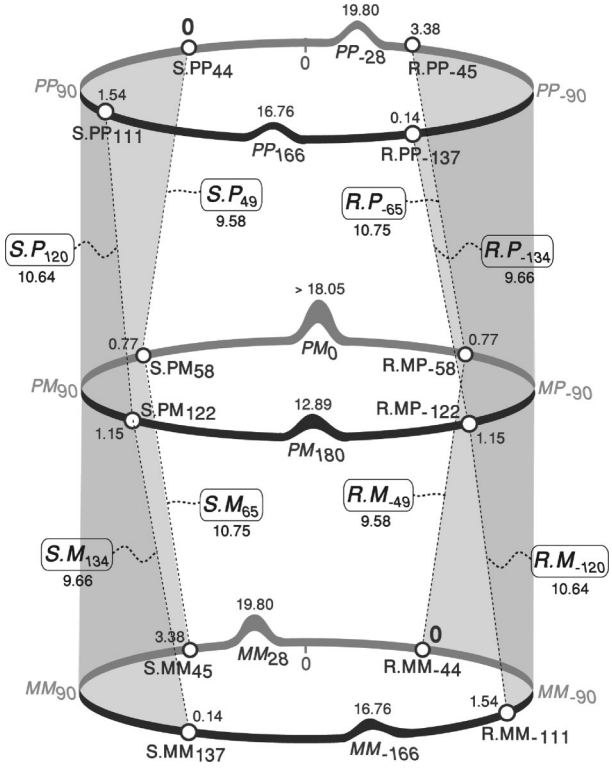

FIGURE 5. Stereodynamics map for bicorannulenyl. Stable conformations are represented by circles. The exact names (which include the DFT calculated dihedral angles) are given for all 12 conformations and 16 transition states. The numbers represent calculated energies in kcal·mol^{-1}, relative to the lowest energy conformation S.PP$_{44}$/R.MM$_{-44}$, at 298.15 K.

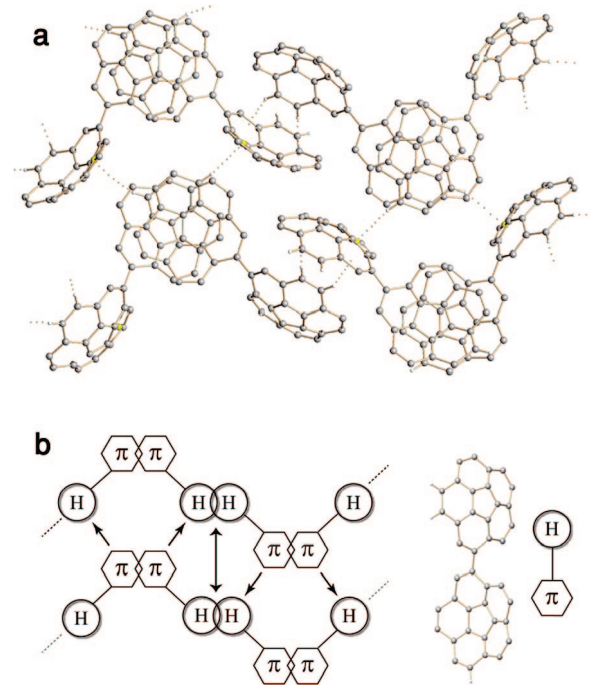

FIGURE 6. (a) A fragment of the solid-state structure of **2** showing a 3D network formed via hydrogen bonding and $\pi-\pi$ interactions. (b) Schematic representation of interactions in the crystal structure of **2**. Overlapping symbols ($\pi-\pi$ and H−H) signify concave-to-convex $\pi-\pi$ interactions and hydrogen bonds, respectively. Single-headed arrows represent additional hydrogen bonds (arrows point toward the hydrogen bond acceptor). Double-headed arrow represents additional, convex-to-convex, $\pi-\pi$ stacking interactions.[16]

for example, is practically observed in the NMR time scale as a direct transition.

The stereochemistry delineated in the map can finally be applied to explain the three NMR absorption sets at low temperatures. The minute energy barriers for conjugation loss allow rapid interchange between "45°"/"135°" conformations even at 190 K. Thus, for instance, S.MM$_{45}$ and S.MM$_{137}$ appear in the NMR as a single averaged S.MM stereoisomer. Hence, the 12 conformations practically represent six stereoisomers, divided into three pairs of enantiomers, which explains the three sets of NMR absorptions when dynamic processes are slowed down.

To further assign the absorptions to structures, the populations of the stereoisomers were determined from the NMR integration ratios. At 190 K, two strong sets of signals and one weak set are seen in relative populations of 69%:28%:3%. Similarly, the calculations, corrected for 190 K, reveal two low-energy diastereomers (S.PP/R.MM and S.MM/R.PP) and a high-energy one (S.PM/R.MP). Their energy differences can be translated into relative populations of 50%:45%:5%. Therefore, the weakest set of signals **c** can be assigned to the S.PM/R.MP diastereomer, and **a** and **b** to S.PP/R.MM and S.MM/R.PP.[21] Symmetry considerations support this assignment, as S.PP/R.MM and S.MM/R.PP possess near-C_2 symmetries, whereas S.PM/R.MP has no apparent symmetry elements.

A comparison of calculated stable geometries and conformations in the crystal demonstrates the difference between gas-phase calculations and the constraints of solid-phase packing. The compound crystallized in the orthorhombic space group *Pbca*, and since this group is centrosymmetric, each diastereomer crystallizes along with its enantiomer in a 1:1 ratio. Two diastereomeric forms of the molecule are present in the crystal in a 70%:30% ratio. Thus, four of the 12 possible conformations of bicorannulenyl are found in the crystal.

The major isomer in the crystal is a "S.PP$_{38}$/R.MM$_{-38}$" pair of enantiomers, which is close in geometry to the S.PP$_{44}$/R.MM$_{-44}$ pair that was found to be the lowest in energy according to the DFT calculation, when corrected to the crystallization conditions (573 K, 1 × 10^{-3} torr). The minor isomer found in the crystal is a "S.PM$_{118}$/R.MP$_{-118}$" enantiomer pair. This pair is close in geometry to the S.PM$_{122}$/R.MP$_{-122}$ pair, which was calculated to lie 1.0 kcal·mol^{-1} higher in energy than the major isomer. Crystal packing forces evidently overcome this minute gas-phase calculated difference. It should be noted that the calculated isomer ratio between the S.PP$_{44}$/R.MM$_{-44}$ and S.PM$_{122}$/R.MP$_{-122}$, corrected for the crystallization temperature, is 34:15%. This ratio is in excellent agreement with the 70%:30% ratio between the "S.PP$_{38}$/R.MM$_{-38}$" and "S.PM$_{118}$/R.MP$_{-118}$" isomers experimentally observed in the crystal.

The solid-state packing of bicorannulenyl involves several different intermolecular interactions, including hydrogen bonding and $\pi-\pi$ stacking (Figure 6). One of the corannulenyl subunits is responsible for the formation of a hydrogen-bonded network, and the other bowl forms aligned stacks based on concave-to-convex $\pi-\pi$ interactions. Two different types of hydrogen bonding are identified, where both concave and convex surfaces serve as acceptors of hydrogen bonds.

(21) The calculated difference in energy between S.PP and S.MM is too small to assign them to (a) or (b) unequivocally. The implications of this vagueness on the actual stereochemical picture are negligible.

In addition, unique convex-to-convex interactions are found in the bicorannulenyl packing pattern. Such interactions, which are obviously a major motif in the crystal packing of fullerenes,[22] have not been observed previously in the crystal packing of corannulene or other known buckybowls. Although they are slightly longer and thus weaker than concave-to-convex $\pi-\pi$ interactions, they are still very well inside the limits set for π-π interactions in benzene dimers.[23] These new interactions apparently contribute additional solid-state packing forces, which bias the crystallization preference toward the $S.PM_{122}/R.MP_{-122}$ isomer over three other diastereomers that are lower in energy according to DFT calculations.

The difference between the two types of bowls in bicorannulenyl is further emphasized by a comparison of single-crystal X-ray diffraction and DFT structural data. Corannulenyl units taking part in the concave-to-convex $\pi-\pi$ stacking exhibit the largest deviations between the crystal and calculated structures. This average difference is 4.2% and 1.3% for bond lengths and angles, respectively, in the major isomer ($S.PP_{44}/R.MM_{-44}$) and 9.6% and 4.6% in the minor ($S.PM_{122}/R.MP_{-122}$). In comparison, the differences in the bowl that interacts chiefly through hydrogen bonding are 0.3−0.4% for bond lengths and angles in both the major and minor isomers.

The important geometrical parameters in **2** are bowl depth[24] and torsion angle, and again the single-crystal X-ray diffraction findings agree well with DFT predictions. Bowl depths in the crystal are within 0.06 Å of the calculated values; torsion angles deviate by only 4.7−6.4°.[16]

The calculated energies of the multiple transition states can be compared to energy barriers obtained from dynamic NMR experiments and to known values of simpler analogues of bicorannulenyl. In biaryls, energy barriers for rotation about the central σ-bond span from 1.5 kcal·mol^{-1} in biphenyl to 45.2 kcal·mol^{-1} in the crowded 9,9′-bianthryl.[25] In bicorannulenyl, the lowest steric-hindrance rotation barrier belongs to PM_{180} (12.9 kcal·mol^{-1}). At this barrier, ϕ equals exactly 180°, and therefore the preferred rotation pathway in **2** is transoid. The same is found for 1,1′-binaphthyl, a smaller analogue that can be mapped onto the bicorannulenyl skeleton.[26] However, rotation is easier in bicorannulenyl than in 1,1′-binaphthyl:[25,27] only 12.9−19.8 kcal·mol^{-1} compared to 22.5−32.4, respectively. This reduction in barrier height can be explained by the curvature of the polycyclic skeletons in **2**, which increases the distance between the colliding hydrogens pairs, thus reducing the steric crowding that gives rise to the barrier.

With respect to the small rotation barriers arising from conjugation loss, bicorannulenyl resembles its analogue 1,1′-biphenyl (which also maps onto its skeleton). These barriers rise to 1−2 kcal·mol^{-1} [18] in both molecules, indicating a similar degree of conjugation. Rotation about a single bond is hardly influenced by conjugation, either in solution or in the gas phase.

Rotations about the σ bond represent one mechanism for the conversion of one diastereomer to another, while bowl inversions represent an alternative. This is best exemplified by interconversions between the two major pairs of enantiomers, S.PP/R.MM ⇌ S.MM/R.PP (signal sets **a** and **b** in the NMR, Figure 1). The stereodynamics map shows how this process can proceed through two alternative pathways: (1) two bowl inversions turn S.PP into S.MM; (2) a single rotation about the σ-bond converts S.PP to R.PP, which is the enantiomer of S.MM.

Since enantiomers exhibit isochronous NMR absorptions, the alternative interconversion pathways between the two major diastereomers would be indistinguishable by NMR. Thus, calculations are needed to determine the preferred route. Our DFT results predict energy barriers of 8.7−10.5 kcal·mol^{-1} for bowl inversions in bicorannulenyl. These values fall within the range of literature barriers for bowl inversion in singly substituted corannulenes (9−12 kcal·mol^{-1})[1] and are 1−2 kcal·mol^{-1} lower than the smallest steric hindrance rotation barrier, suggesting that bowl inversions rather than bond rotations are the preferred pathway for interconversion between the major isomers.

To further characterize the stereodynamics in the molecule, the exchange rates of the three diastereomers were experimentally measured by exchange spectroscopy (EXSY-NMR), and the energy barriers were extracted using the Eyring equation.[16] The experimental energy barriers span a range from 12.0 to 13.1 kcal·mol^{-1}, slightly higher than the known literature range for bowl inversion in singly substituted corannulenes.[1] The nearly systematic difference of $+3 \pm 1$ kcal·mol^{-1} between the experimental and calculated values may be attributed to the difference between gas-phase calculations and solution-phase barriers at 190 K and to imperfection of the computational model.

The blank spots on the stereodynamics map are finally colored, as the result of a fertile interplay between theory and experiment. When cooling a solution of **2**, rotation about the central bond is first to slow down, separating the six diastereomers into two groups: three right-handed and three left-handed helical conformations, where the conformers of each group still interconvert through bowl inversions. Upon further cooling, bowl inversions freeze as well, overall resulting in the line splitting observed in Figure 1 below 250 K.

It is interesting to note that all 12 conformers of **2** are chiral and, additionally, that 18 out of the 20 transition states are chiral (i.e., all 8 bowl inversion barriers, all 6 conjugation loss barriers, and 4 out of 6 steric hindrance barriers are chiral). Most enantiomerization pathways are thus chiral all the way through. Such chiral enantiomerizations contain a curious point of latent handedness,[28] where the structure is chiral but its handedness cannot be determined. It should be noted, however, that of the two achiral transition states, namely PM_0 (C_s) and PM_{180} (C_i), the latter is the lowest energy steric hindrance barrier for bond rotation. Since all enantiomerization pathways must pass through at least one steric hindrance barrier, the kinetically favored enantiomerization pathway for each pair of enantiomers is actually the one that involves an achiral transition state (PM_{180}).

Overall, bicorannulenyl demonstrates how the introduction of a biarylic structural element brings about complex stereodynamics to the corannulene family. A radical example for the rich stereochemistry of oligocorannulenes is another molecule

(22) Tsuzuki, S.; Uchimaru, T.; Tanabe, K. *J. Phys. Chem. A* **1998**, *102*, 740.

(23) (a) Sinnokrot, M. O.; Sherrill, C. D. *J. Phys. Chem. A* **2006**, *110*, 10656. (b) Janowski, T.; Pulay, P. *Chem. Phys. Lett.* **2007**, *447*, 27.

(24) The bowl depth is defined as the average distance between the 10 rim carbons and the plane defined by the central pentagon.

(25) Nori-Shargha, D.; Asadzadeha, S.; Ghanizadehb, F.-R.; Deyhimic, F.; Aminic, M. M.; Jameh-Bozorghia, S. *J. Mol. Struct. (THEOCHEM)* **2005**, *717*, 41.

(26) Kranz, M.; Clark, T.; Schleyer, P. v. R. *J. Org. Chem.* **1993**, *58*, 3317.

(27) (a) Cooke, A. S.; Harris, M. M. *J. Chem. Soc. C* **1963**, 2365. (b) Colter, A. K.; Clemens, L. M. *J. Phys. Chem.* **1964**, *68*, 651.

(28) Avnir, D.; Katzenelson, O.; Keinan, S.; Pinsky, M.; Pinto, Y.; Salomon, Y.; Zabrodsky Hel-Or H. In *Concepts in Chemistry: A Contemporary Challenge*; Rouvray, D. H., Ed.; Research Studies Press: Taunton, England, 1996, pp 283−324.

from our laboratory, 1,3,5,7,9-pentacorannulenyl-corannulene, featuring no fewer than 1120 distinct conformations, or 280 stable pairs of enantiomers.

In addition to the stereodynamics, the biaryl motif should also influence the electronic behavior of bicorannulenyl. This behavior should come into play, for example, when the molecule is reduced with alkali metals, facilitating phenomena such as electron hopping, supramolecular aggregation, and reductive ring closure. We have already started investigating the anions of bicorannulenyl, and a unique reduction profile is beginning to materialize.

Experimental Section

Synthesis. Bicorannulenyl was first prepared more than 10 years ago,[29] and preliminary investigations into its reduction with alkali metals were reported soon thereafter.[30] It has subsequently been synthesized also by others.[31] The procedure used here was modeled after that reported by Rawal and co-workers.[32]

Into a 10 mL Schlenk flask with a stir bar were added 600 mg (1.82 mmol) of bromocorannulene, 0.100 g (0.912 mmol) of hydroquinone, and 0.594 g (1.82 mmol) of cesium carbonate. The flask was then purged with nitrogen. Into a heat-dried 5 mL cone bottom flask with a stir bar were added 22.2 mg (0.0729 mmol) of tri-*o*-tolylphosphine and 16.4 mg (0.0729 mmol) of palladium acetate. This flask was also purged with nitrogen. To each flask was added 1.95 mL of dimethylacetamide, and the contents of both flasks were stirred briefly. The catalyst solution was then transferred to the Schlenk flask by syringe. This mixture was lowered into a preheated silicon bath at 100 °C and stirred for 24 h under a nitrogen atmosphere. The reaction mixture was run through a plug of silica with excess methylene chloride and washed once with a 10% HCl solution. The organic layer was then dried with magnesium sulfate and filtered. The solvent was removed under reduced pressure, and the crude products were purified on a column of silica with a 1:19 methylene chloride/cyclohexane solvent system to give a pale yellow to white solid (yield 97 mg, 21.3%), mp 160−162 °C. Very significant amounts of bromocorannulene and corannulene were also recovered. MS *m*/*z* (relative intensity): 498 (M^+, 100), 249 (46), 248 (63), 125 (7), 42 (37). HRMS, calculated for $C_{40}H_{18}$ (M+): 498.1408, found 498.1407. ^{1}H NMR (400 MHz, THF-d_8, 320K) δ 8.18 (s, 1H, H_2), 7.96 (d, $J_{H,H}$ = 8.81 Hz, 1H), 7.92 (d, $J_{H,H}$ = 9.16 Hz, 1H), 7.90 (d, $J_{H,H}$ = 10.00 Hz, 1H), 7.87 (d, $J_{H,H}$ = 9.21 Hz, 1H), 7.86 (d, $J_{H,H}$ = 9.25 Hz, 1H), 7.80 (d, $J_{H,H}$ = 8.43 Hz, 1H), 7.70 (d, $J_{H,H}$ = 8.77 Hz, 1H), 7.66 (d, $J_{H,H}$ = 8.79 Hz, 1H) ppm. ^{1}H NMR (400 MHz, THF-d_8, 190K) δ 8.32 (s, 1H, a, H_2), 8.50 (d, $J_{H,H}$ = 10.09 Hz, 1H, c), 8.49 (s, 1H, c, H_2), 8.30 (d, $J_{H,H}$ = 8.71 Hz, 1H, b), 8.29 (d, $J_{H,H}$ = 8.72 Hz, 1H, a), 8.21 (d, $J_{H,H}$ = 9.08 Hz, 1H, c), 8.17 (s, 1H, b, H_2), 8.16 (d, $J_{H,H}$ = 8.96 Hz, 1H, a), 8.10−8.06 (m, 4.85H, b+c), 8.04 (d, $J_{H,H}$ = 8.96 Hz, 1H, a), 8.00 (d, $J_{H,H}$ = 8.65 Hz, a), 7.91 (d, $J_{H,H}$ = 8.69 Hz, 1H, a), 7.72 (d, $J_{H,H}$ = 8.96 Hz, 1H, b), 7.54 (d, $J_{H,H}$ = 9.25 Hz, 1H, c), 7.42 (d, $J_{H,H}$ = 8.93 Hz, 1H, a), 6.69 (d, $J_{H,H}$ = 9.21 Hz, 1H, c) ppm. ^{13}C NMR (400 MHz, THF-d_8, 320K) δ 139.22, 136.21, 136.07, 136.98, 135.72, 135.47, 135.44, 131.23, 131.19, 131.14, 130.95, 130.94, 128.43, 127.31, 127.22, 127.12, 127.01, 126.98, 126.97, 126.82 ppm. ^{13}C NMR (400 MHz, THF-d_8, 190K) δ 139.07, 138.67, 136.61, 136.14, 136.01, 135.96, 135.80, 135.69, 135.65, 135.33, 135.20, 135.13, 131.66, 131.54, 131.31, 131.24, 131.03, 130.38, 129.83 (C_2), 128.00, 127.83, 127.70, 127.62, 127.43, 127.42, 127.20 ppm.

DFT Calculations. All DFT calculations described herein were carried out using the GAUSSIAN 03 program package.[20] The PBE0 functional[33] was employed with the 6-31G* basis set, and energies were corrected for zero-point and Gibbs free energy at 298 K (unless stated otherwise).

Crystallographic Procedure. Crystals of bicorannulenyl ($C_{40}H_{18}$, **2**) suitable for the single-crystal diffraction study were grown by deposition from the gas phase over 2 weeks at 300 °C. At temperatures higher than 310 °C traces of decomposition were observed. An X-ray data set for **2** was collected on an X-ray diffractometer equipped with graphite-monochromated Mo Kα radiation (λ = 0.71073 Å). The structure was solved by direct methods and refined against F^2 by the full-matrix least-squares technique. Data were corrected for absorption effects using the empirical methods SADABS. The molecule exhibits a half-molecule diastereomeric disorder so only one-half of all carbon atoms were refined anisotropically. All hydrogen atoms were included at idealized positions for structure factor calculations.

Acknowledgment. We express our gratitude to Dr. David Danovich and Elina Ploshnik for vital help with the calculations, and Prof. Silvio Biali for fruitful discussions. Financial support from the National Science Foundation (NSF) and from The Lise Meitner-Minerva Center for Computational Quantum Chemistry is gratefully acknowledged.

Supporting Information Available: Clarification of bicorannulenyl's nomenclature, conformational space scan procedure, DFT calculated structures and energies of all species with thermodynamic corrections, comparison between EXSY and DFT barriers, single-crystal analysis, and comparison between X-ray and DFT geometries, including CIF file. This material is available free of charge via the Internet at http://pubs.acs.org.

JO800359Z

(29) Cheng, P.-C. Corannulene: Novel synthesis and reactions. Ph.D. dissertation, Boston College, Chestnut Hill, MA, 1996.

(30) (a) Shabtai, E.; Weitz, A.; Rabinovitz, M.; Cheng, P.-C.; Scott, L. T. Charged Extended Corannulenes, 62nd Meeting of the Israel Chemical Society, February 1997; abstract no. B68. (b) Benshafrut, R.; Shabtai, E.; Rabinovitz, M.; Scott, L. T. *Eur. J. Org. Chem.* **2000**, 1091.

(31) Elliott, E. L. The synthesis and properties of corannulenes and novel corannulene derivatives. Ph.D. dissertation, University of California, San Diego, La Jolla, CA, 2004.

(32) Hennings, D. D.; Iwama, T.; Rawal, V. H. *Org. Lett.* **1999**, *1*, 1205.

(33) Adamo, C.; Barone, V. *J. Chem. Phys.* **1999**, *110*, 6158.